A three-stage method for the 3D reconstruction of the tracheobronchial tree from CT scans

Jan Rosell[a], Paolo Cabras[a,b]

[a] *Institute of Industrial and Control Engineering (IOC), Universitat Politècnica de Catalunya (UPC), Barcelona, Spain.*
[b] *Control, Vision and Robotics Lab, Université de Strasbourg, France.*

Abstract

This paper proposes a method for segmenting the airways from CT scans of the chest to obtain a 3D model that can be used in the virtual bronchoscopy for the exploration and the planning of paths to the lesions. The method is composed of 3 stages: a gross segmentation that reconstructs the main airway tree using adaptive region growing, a finer segmentation that identifies any potential airway region based on a 2D process that enhances bronchi walls using local information, and a final process to connect any isolated bronchus to the main airways using a morphologic reconstruction process and a path planning technique. The paper includes two examples for the evaluation and discussion of the proposal.

Keywords:
Airway segmentation, virtual bronchoscopy, region growing, bronchi wall detection, path planning.

1. Introduction

Bronchoscopy is an interventional medical procedure used to analyze the tracheobronchial tree, mainly to obtain samples from a specific lung site identified by chest X-ray computed tomography (CT) for the diagnosis of lung cancer. The planning of the path to the lesion is usually done on 2D images, which is difficult, error prone and may result in long execution times of the bronchoscopy. Virtual Bronchoscopy (VB) can improve this. VB it is a computer-generated 3D reconstruction that allows medical staff to explore interactively the tracheobronchial tree and also automatically obtain a path to the lesion. Recent clinical studies [1] have proved that VB navigation system shortens the examination and operation times.

A key point in VB is, therefore, the reconstruction of a 3D model of the tracheobronchial tree from the CT scans. Since manual segmentation is prohibitively time consuming, automatic or semi-automatic methods are necessary, which poses a difficult and challenging problem. The difficulty arises because it is not easy to implement efficient and flexible algorithms to cope with all possible clinically relevant cases. Bronchi appear on CT images as dark regions (airway lumen) surrounded by a clear region (the airway wall), but, due to noise, low definition scanner or interpolation artifacts for small-diameter segments, their radio-density vary across the image, and therefore it is not possible to define a global threshold to segment them all. Moreover, the completeness of the reconstruction is becoming even more important now that the new ultra-thin bronchoscopes permit exploration through bronchi as small as 2 mm in diameter.

1.1. Related work

Since the early nineties, several approaches have been proposed to solve the airway segmentation and reconstruction problem. The most common are those based on region growing, on mathematical morphology and on multi-rule or fuzzy logic using anatomical knowledge.

Region growing is a procedure that groups pixels or subregions into larger regions based on predefined criteria [2, chap. 10]. This technique is maybe the most used in the field of airway segmentation and many algorithms often include a region-growing phase. The most common method locates the seed at the beginning of the trachea and grows the region based on voxel connectivity and on a threshold of the HU[1] values. Despite of its simplicity and velocity, 3D region growing suffers from partial volume effects and noise, since it is based on a global threshold used during the segmentation, and the "optimal" threshold for big airway differs a lot from the one required for small airways. The use of an inappropriate threshold may result in the occurrence of parenchyma leakages, mainly in noisy or low-contrasted images. A global threshold may be determined either manually [3] or automatically, based, for instance, on a repeated segmentation process [4]. Other alternatives propose the subdivision of the image in diferent regions, sometimes called volumes of interest, where the threshold is locally adapted [5, 6, 7]. The occurrence of leakages can also be reduced if algorithms to detect bronchi walls, as that proposed in [8], are used as a pre-processing step.

Airway segmentation methods using *mathematical morphology* [9] are also very common. These methods usually start searching for candidate airways using binary or gray-scale morphologic operations and, then, exclude the false candidates with a 3D reconstruction or analyzing the 3D relationships and shape properties [10]. These techniques are also combined with region growing methods, i.e. a first region growing step is performed to segment the trachea and biggest bronchi and then

[1] HU stands for Hounsfield Units, that is the scale that measures the radio-density. The darker voxels correspond to the air, that has a value of -1000 HU.

a second step copes with the segmentation of finer bronchi using the morphological gradient (the difference between 3D greyscale dilation and 3D greyscale erosion) [11], or using a morphological filtering based on a closing with structure elements of different sizes, and a reconstruction applied to all slices in all the three planes: axial, sagittal and coronal [12].

Rule-based or fuzzy logic methods have also been proposed, which allow the use of anatomical knowledge of the airway tree. For instance, [13] described a rule-based method based on a combination of 3D seeded region growing that is used to identify large airways, rule-based 2D segmentation of individual CT slices to identify probable locations of smaller diameter airways, and merging of airway regions across the 3D set of slices. The work in [14] refined the method of [13] improving the specificity of the rules introducing fuzzy logic techniques. Fuzzy logic has also been used in [15] and [16] to define a multiseeded fuzzy connectivity functions to segment voxels as lumen or wall, using different affinity relations like homogeneity-based affinity to detect similarity of intensity values over a neighborhood, or directional affinity to indicate the growing direction of the airway being reconstructed.

Many of the previous methods and techniques described above result in the main airway tree plus isolated non-connected branches. Therefore, some approaches include a final connection step. For instance, in [17] tubular structures are detected in the data volume and then the different structures are connected together according to branching angle (angle between the central axis of the two branches), branch radius and distance. A more sophisticated and precise method [18] searches for new candidates, calculates the cross sectional surfaces of the branches and connects the disjoint branches minimizing a connection cost based on the directions of the branches to be connected, the gray values of the voxels and other specific characteristics. The connection is made interpolating the cross sectional surfaces.

The topological and geometrical correctness has also been tackled, like the work in [19] that presents a method to guarantee that airway segmentations do not have loops or invalid voxel-to-voxel connections, or the work in [20] that presents an algorithm where surface patches are constructed adaptively based on the number of elemental points, leading to to the elimination of geometrical distortions usually occurring at small bronchi.

1.2. Proposal Overview

The paper presents a method for the 3D reconstruction of the tracheobronchial tree from the chest CT images that, after the selection of the lung region and the performance of some basic filtering, is organized in three stages:

1) A first stage, called *raw segmentation*, devoted to segment the biggest airways using a region growing method with adaptive thresholds.

2) A second stage, called *fine segmentation*, devoted to detect any small region that can be segmented as airways based on a 2D process that first enhances bronchi walls using local information, and then executes a basic segmentation and filtering process.

3) A third stage, called *reconstruction*, devoted to connect any isolated bronchus to the main airways. It first uses a morphological reconstruction process, and then a procedure based on a path planning technique considering proximity and directional information as well as the gray values of the image.

The proposal is framed within a VB system described in [21], that permitted a guided navigation using a haptic device. The system included three main modules: a simple reconstruction module based on morphological processing to obtain a 3D model of the airways, a path planning module to find a path from the trachea to the lesion taking into account the geometry and the kinematic constraints of the bronchoscope and detailed in [22], and a navigation module using a haptic device that receives guiding forces to follow the computed path and whose movements are constrained to mimick those allowed by the bronchoscope. The present paper is a new proposal for the reconstruction module, able to segment thinner bronchi and obtain a more complete model of the tracheobronchial tree in order to make the haptic-based VB system apt to simulate ultrathin bronchoscopies.

The paper is structured as follows. Section 2 describes the pre-processing step to select the lung region and Sections 3, 4 and 5 describe, respectively the three stages of the proposal. Finally Section 6 presents some examples and evaluates and discusses the contribution.

2. Pre-processing

In order to reduce the processing time, the airway reconstruction algorithm must be focused only on the lung region, i.e. all other parts found in the chest CT data must be cleared off. This is done with a mask applied to the original CT data (Fig. 1a), and that is computed as follows. The darkest part of the original CT image is first obtained with a binarization operation using a threshold between the minimum value of the image (i.e. -1000 HU that correspond to the air) and -200 HU. As a result, the lung region as well as those air regions exterior to the body are segmented (Fig. 1b). After an opening operation that eliminates little regions due to noise (Fig. 1c), the lung component is recovered by a binary reconstruction operation from a seed located at a point at the beginning of the trachea (Fig. 1d). Finally, a closing operation with a big structuring element is performed to close those holes corresponding to those structures inside the lung but not selected due to the threshold operation (Fig. 1e). The obtained image is the mask used to recover all the original gray values of the whole lung region of the initial data set (Fig. 1f). The pixels not belonging to the selected lung region are labeled as background and will be not considered in the next stages, shortening the computing time.

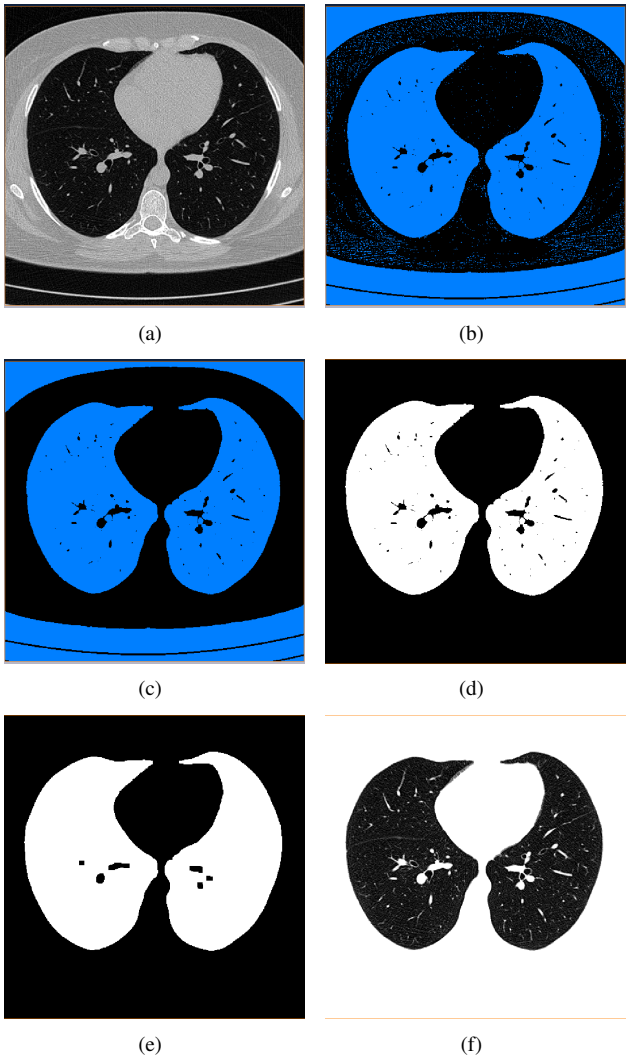

Figure 1: Lung region selection steps: (a) the original data set with all the chest internal structures; (b) binarization; (c) filtering; (d) reconstruction of central part; (e) obtained mask; (f) masked original image.

3. First stage: Raw Segmentation

The aim of this stage is to segment the biggest airways, which are easier to detect because of their dimensions, the thickness of their walls and the more homogeneous gray-scale values. The procedure is a region growing with an adaptive threshold to control parenchyma leakages. A marker image is initialized with a mark at the beginning of the trachea, and an upper threshold (Upp) is set to -700 HU, then the following two steps are interleaved until no growing occurs (i.e. until the volume of the marker image being grown keeps unchanged):

1. *Growing step*: Grows the marker image and computes the increase in volume. The procedure:
   - Dilates the marker image by 1, with a 6-neighborhood, and uses it to mask the original CT image.
   - Binarizes the masked image between -1000 HU and Upp and then makes a morphologic closing operation. The result is the new marker image.
   - Computes the resulting volume increase, ΔV_i.
2. *Leakage control step*: Verifies if the ratio of volume increase is above a given threshold, indicating that a leakage is occurring. The procedure:
   - Computes the explosion parameter as:
   $$e = \frac{\Delta V_i - \Delta V_{i-1}}{\Delta V_{i-1}} 100 \quad (1)$$
   - Verifies if $e > E$ and if this is the case then steps back to the *Growing step* (deleting the last growth), and decreases the upper threshold, i.e. $Upp = Upp - \delta$, to grow in a more conservative way the next time.

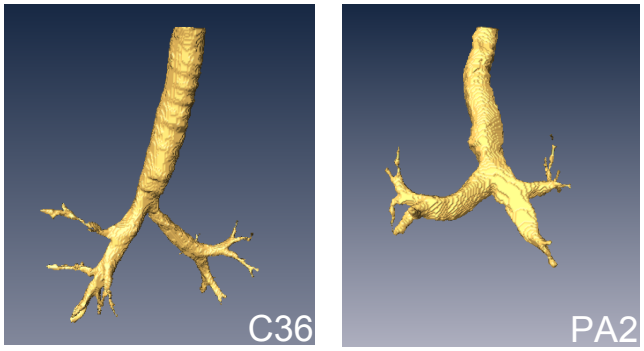

Figure 2: Result of the raw segmentation stage.

The value of E has been experimentally evaluated for several data, being a value in the range $[4.5, 5]$ a general good option. Smaller values of E result on a more conservative behavior that gives rise to a smaller reconstructed volume; higher values may result in the occurrence of leakages. The value of δ is the threshold discretization step; it is not a critical value and it is currently set at $\delta = 15$ as a good trade-off between accuracy and computational cost.

This step is not critical because, on the one hand, if it is too conservative, those voxels that could have been segmented as airways using other values are actually segmented in stage 2. On the other hand, some small leakages may not be detected because their growing is below the threshold, but in this case the badly segmented voxels are usually eliminated in the reconstruction step in stage 3.

As an example Fig. 2 shows the results obtained after applying the first stage to two cases, called C36 and PA2, that will be used throughout the paper. It can be observed that the main branches of the tracheobronchial tree have been reconstructed.

4. Second stage: Fine Segmentation

Once the biggest airways have been detected in the first stage, the algorithm focuses on the segmentation of the smallest bronchi. The proposal centers the attention in identifying bronchi wall pixels and follows some ideas presented in [8]. The proposal has the following four steps (further detailed in the subsections):

1. *3-grade segmentation step*: This step makes a 2D processing of pixels one by one, excluding those pixels which were labeled as airway lumen in the first stage. Since the airway walls and vessels can be distinguished in the image for their higher brightness with respect to the rest of the lung, each pixel is compared with its neighborhood and, according to that, one of the following "grades" are assigned to it:
   - Grade 2: when the pixel is brighter than the surrounding pixels (it is a *bronchi wall or vessel pixel*).
   - Grade 1: when the pixel is not clearly darker nor brighter than the surrounding pixels (it is an *uncertain pixel*).
   - Grade 0: when the pixel is darker than the surrounding pixels (it is an *airway pixel*).
2. *Wall repair step*: Since the previous step may end with incomplete bronchi walls, i.e. with some wall pixels labeled with grade 0, this step first detects those pixels where a bronchi wall seems to be broken (i.e. those that satisfy a given pattern) and then connect two of them if they are close enough (marking with grade 1 those pixels which connect them).
3. *Decide step*: A third step disambiguates the uncertainty of pixels with grade 1 using intra-slice information.
4. *Segmentation and filtering step*: A final step enhances, on the pre-processed input image, the gray-level of the pixels graded as walls and then binarizes the resulting image to segment the airways region, excluding those areas that are too small (noise) or too large (parenchima).

4.1. 3-grade segmentation step

To determine the grade of a pixel, a set of segmentation functions are computed on a set of six line projections defined within a box centered at the pixel. Let p be a pixel of an axial plane of the CT image and I_p be a 100×100 window centered at p. Then, a projection $P_\alpha(p)$ is defined as the set of pixels (excluding p) that conform a (straight) line that passes by p forming an angle α with the horizontal axis, and a segmentation function $s(P_\alpha(p))$ is defined weighting the mean, the minimum value and the mid-point value of the pixels in $P_\alpha(p)$:

$$\begin{aligned} s(P_\alpha(p)) \quad = \quad & a \cdot \text{mean}(P_\alpha(p)) + b \cdot \min(P_\alpha(p)) + \\ & + c \cdot \tfrac{1}{2}(\max(P_\alpha(p)) + \min(P_\alpha(p))), \end{aligned} \tag{2}$$

with a, b and c fixed at $a = 0.45$, $b = 0.35$ and $c = 0.2$.

For each pixel, a set of six random projections are used with angles (in degrees) equal to $\alpha_i = 30i + \beta$ with i an integer value in the range $[0, 5]$ and β a random real value in the range $[0, 30)$. The function $grade(p)$, shown below, applies the segmentation function $s(P_\alpha(p))$ to each projection and compares the result with the gray value of p. If in all six cases the gray value of p is greater than $s(P_{\alpha_i}(p))$, then p can be considered a bronchi wall ($grade(p) = 2$); if the gray value of p is grater than $s(P_{\alpha_i}(p))$ in only three or less cases, then p is considered airways ($grade(p) = 0$); otherwise it is uncertain ($grade(p) = 1$), i.e.:

$$grade(p) = \begin{cases} \mathbf{2} & \text{if } I_p(p) > s(P_{\alpha_i}(p)) \ \forall i \in [0,5] \\ \mathbf{0} & \text{if } I_p(p) > s(P_{\alpha_i}(p)) \text{ in less than 4 directions} \\ \mathbf{1} & \text{otherwise} \end{cases} \tag{3}$$

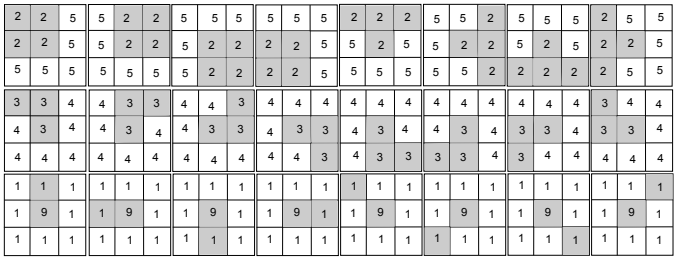

Figure 3: Weight patterns to detect border pixels: If these values are masked by the pixels shown in gray and summed, the result is either 8, 9 or 10, indicating that the pixel in the center is a potential border pixel.

Several window sizes have been tested, being the selected one a good compromise between computational cost and the capacity to capture the gray-level values of a big neighborhood of a pixel. Also, several values for a, b and c have been tested on several chosen regions; the selected values gave good results, although these values are not critical.

4.2. Wall repair step

In low-contrasted parts it may happen that the grades labelization process does not detect all the wall pixels and, then, some bronchi wall result to be incomplete. To compensate this behavior, an automatic step is done to repair the wall by connecting close pixels, called border pixels, where a wall seems to be broken. Border pixels are detected as follows. Let M_p be a 3×3 binary mask centered at p such that $M_p(q) = 0$ if $grade(q) = 0$ and $M_p(q) = 1$ otherwise, and let A_i $i = 1..24$ be the set of weight patterns shown in Fig. 3. If the result of summing the nine values of the pixels after masking A_i by M_p equals 8, 9 or 10, then pixel p is selected (this will happen when the non-zero values of M_p correspond to those pixels shown in gray in Fig. 3). Any pair of selected pixels that are less than 5 pixels apart, are considered border pixels (Fig. 4b) and are connected by setting to grade 1 all those pixels that lie on the segment between them (Fig. 4c).

4.3. Decide step

The third step of this stage is to disambiguate the unresolved pixels (those with grade 1). This is done using intra-slice information, i.e. looking the grades of the pixels on the neighbor slices. A *decide* function is defined to look, for each pixel p with grade 1, the grades of the pixels above and below it (p_a and p_b) and the 4-neighbors of p_a and those of p_b in the corresponding slices. The grade of p is changed to 2 (i.e. to a wall pixel) if at least two of the observed pixels (one from the slice above and one from the slice below) have grade 2, otherwise it is set to grade 0. Fig. 4d shows the results of the decide step,

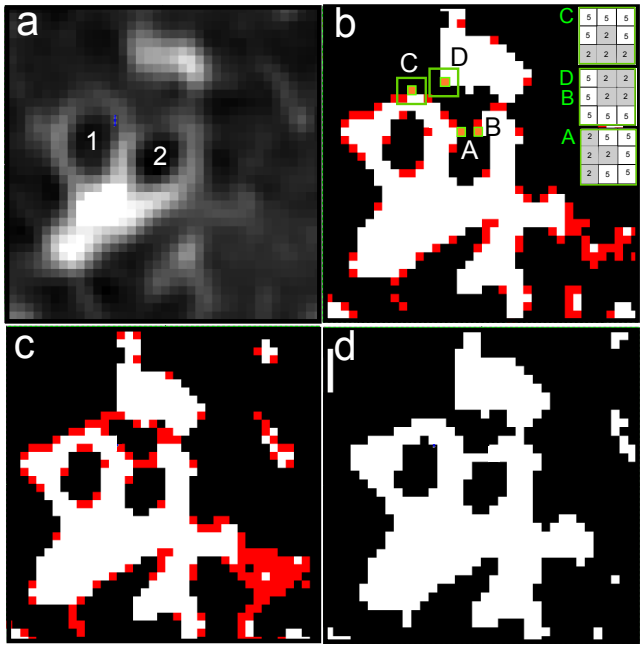

Figure 4: a) Part of a CT slice with two bronchi; b) Segmented pixels (grade 0 in black, grade 1 in red, grade 2 in white) and two pairs of border pixels A-B and C-D (in orange) and the masks used to identify them; c) As a result of the connection process, the pixels connecting the pairs of border pixels have been set with grade 1 and are shown in red; d) Final decide step using intra-slice information: the pixels closing the wall of bronchus 2 have correctly changed to grade 2 and shown in white; other uncertain pixels have correctly been changed to grade 0 and are shown in black.

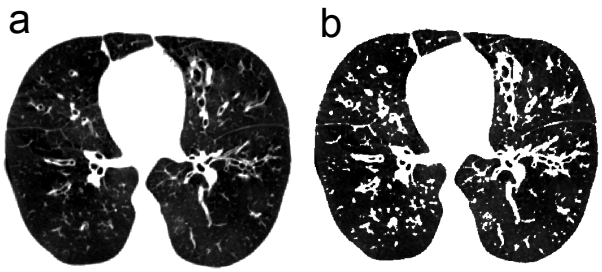

Figure 5: a) Original image; b) Image with enhanced walls.

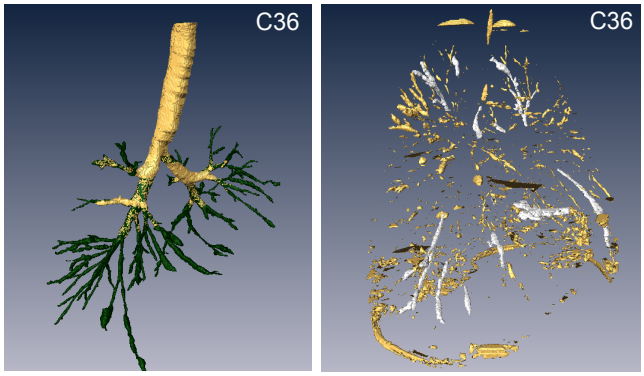

Figure 6: The regions segmented as airways in stage 2 can be divided into those that are already connected to the main tree (green region on the left) and the isolated ones (right). Those isolated regions that pass the shape and position filtering are painted in white.

that changed to grade 2 some of the uncertain pixels of the wall of bronchus number 2, allowing to close the wall, and to grade 0 some others.

4.4. Segmentation and filtering step

The last step consists in first modifying, in the original image, the gray value of the pixels labeled as walls, by increasing their HU value. As an example, Fig. 5a shows a slice of the original image and Fig. 5b the image with the enhanced walls that allow to isolate the airways regions. Then, the image is binarized between -1000HU and -700HU and the result filtered to eliminate regions that are too small (noise) or too big (parenchima), using first an area filter, slice by slice, and then a volume filter. The resulting regions are considered airway regions.

5. Third stage: Reconstruction

The reconstruction is devoted to merge the segmentation results of the two first stages. This is done in two steps:

1. *Binary reconstruction step*: A binary image is built with all the voxels segmented as airways in the first two stages. Then, a binary reconstruction is launched from a seed in the trachea. The result is the main airway tree found in stage 1 extended with the voxels segmented as airways in stage 2 and that are already connected to it (Fig. 6 left).
2. *Connection step*: All those voxels segmented as airway in stage 2 but not connected to the main airway tree conform the isolated airway regions (Fig. 6 right). This step tries to connect them to the airway tree as follows:
   (a) Interruption points detection: The points where the branches of the main airway tree end are detected.
   (b) Shape and position filter: Regions with a tubular shape are characterized by having the first eigenvalue, λ_1, resulting from the principal component analysis (PCA) applied to their voxels, much larger than the other two, λ_2 and λ_3. Therefore, those regions where the first two eigenvalues are similar ($\lambda_1/\lambda_2 < 2$) are discarded. Also, since this stage tries to reconstruct broken bronchi, all those regions that do not lie within a small neighborhood of the interruption points are discarded too, because they may not be part of the interrupted bronchi (this small neighborhood has been defined with a $20 \times 20 \times 20$ box, called neighboring box, that allows to reconstruct gaps up to approximately 0.7cm). The regions that pass the shape and position filtering are called floating branches (white regions in Fig. 6 right).
   (c) Connection process: The interruption points are connected to the floating branches using path planning techniques as detailed below.

As an example, Fig. 7(top) illustrates the result of the binary reconstruction step for cases C36 and PA2, and Fig. 7(bottom)

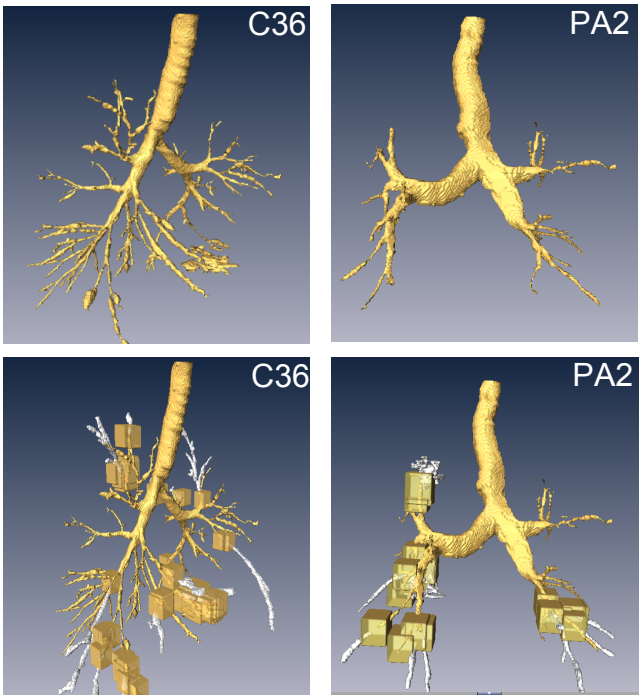

Figure 7: Top row: main trees after the extension; Bottom row: floating branches (in white) to be connected to the main trees at the interrupt points located at the center of the boxes.

the floating branches (in white) to be connected to the main trees at the interrupt points located at the center of the boxes.

Path planning is a discipline in robotics devoted to the computation of collision free paths for a robot from an initial to a final configuration. Some approaches discretize the space and compute a potential field on a grid, with a global minima at the goal cell. Then the planning is reduced to the following of the negated gradient of the potential field. One example is the navigation function NF1 [23] that is obtained by computing the L1 distances from the goal cell by a wavefront propagation.

The connection process detailed here is a simpler and more robust variant of the procedure presented in [24]. It uses a path planning technique based on a modulation of the NF1, called *connection NF1*. This modulation makes the propagation more easy (by setting a lower potential value) along the direction of the interrupted branch and along darker voxels (i.e. those more prone to be airway voxels). For each interruption point, the *connection NF1* function is computed inside the neighboring box centered at the point, provided that a floating branch partially lies within the box. The computation is done as follows: the potential of all the voxels of the neighboring box is initialized to a high value, except for the voxel corresponding to the interruption point that is set at a zero potential; then, starting at the interruption point, the potential is iteratively propagated from one voxel to its 6-neighbor voxels with the following expression:

$$\begin{aligned} d_j &= \min\{d_j^0, d_i + \Delta\} \\ \Delta &= 1 - \omega_G k_G - \omega_\theta k_\theta > 0 \end{aligned} \tag{4}$$

where:

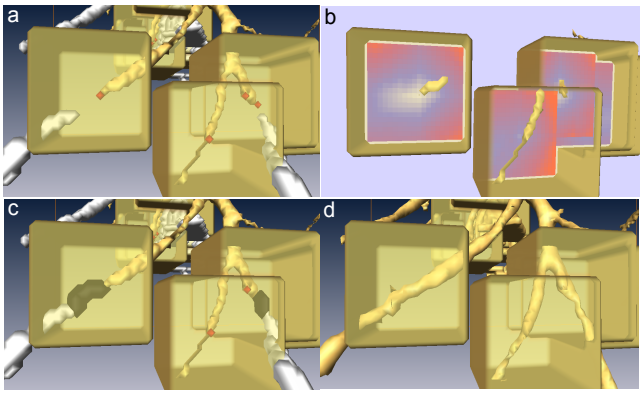

Figure 8: a) Neighboring boxes centered at the interruption points (in red) and the interrupted and floating branches to be connected; b) Values of the NF1 connection function shown in colors for a given plane; c) Connection path found following the negated gradient of the NF1 function; d) Reconstructed bronchi.

- d_i and d_j are the potential values of two neighbor pixels, and d_j^0 is the value of d_j prior to the propagation of the potential from d_i.
- k_G is a value in the range $[0, 1]$ that modulates the propagation as a function of the gray level of the considered voxel:

$$k_G = \frac{Gray(p_i)}{\min_{\forall p \in Box(p_i)} Gray(p)} \tag{5}$$

  i.e. the ratio between the gray level of the voxel and the minimum gray value of the data set. Darker voxels result in a higher value of k_G and thus in a lower value of the potential d_j.
- k_θ is a value in the range $[-1, 1]$ that modulates the propagation as a function of the angle θ between the direction of the interruption branch and the vector from the interruption point to the voxel where the potential is being computed:

$$k_\theta = \begin{cases} -1 & \text{if } \cos(\theta) < 0 \\ \cos(\theta) & \text{otherwise} \end{cases} \tag{6}$$

  Voxels around the direction of the interrupted branch result in a higher value of k_θ and thus in a lower value of the potential d_j.
- ω_G and ω_θ are positive weights satisfying $\omega_G + \omega_\theta = W$ with $0 < W < 1$. Considering this constraint and the ranges of k_G and k_θ, the value of Δ satisfies $\Delta > 0$, which guarantees that the potential function has a unique minimum at the interruption point. The value of W has been chosen to be 0.98, although the exact chosen value is not critical.

Using the propagation described by Eq. (4), the minimum value is set at the interruption point and the potential value has a monotone increase, with a minor slope through darker voxels located around the direction defined by the interrupted branch.

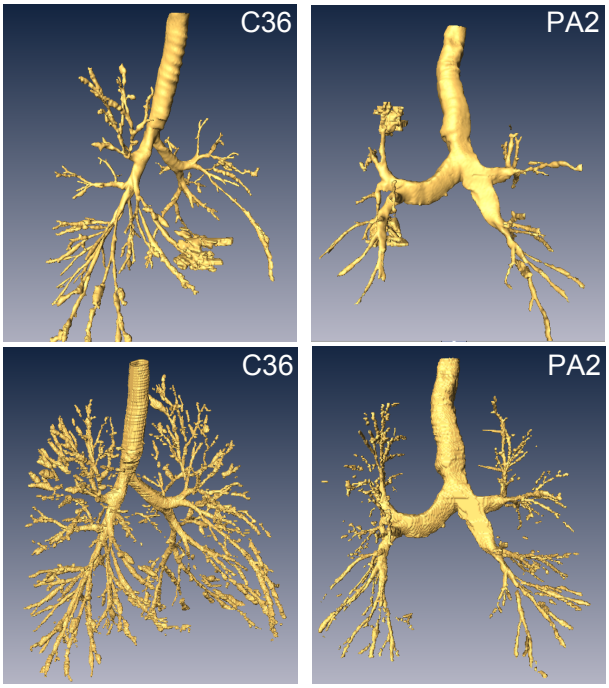

Figure 9: Final 3D models (top) and corresponding ground truths obtained by a manual segmentation process (bottom).

Once the *connection NF1* values are computed, the connection between the main airway tree and the floating branches is done with the following steps for each interruption point:

- From the floating branches within the neighborhood box, select the point with lowest potential.
- From that point follow the negated gradient of the potential function until the interruption point (that has zero potential) is reached.
- Dilate the channel of cells and label the result as airways.

As an example Fig. 8 illustrates the process to connect interruption points with floating branches using the connection NF1 function computed in the neighboring boxes.

6. Evaluation and discussion

6.1. Examples

Two datasets have been used to illustrate our proposal, named C36 and PA2. The final reconstructed models are shown in Fig. 9 (top). Dataset C36 has been selected from the testing CT datasets provided by the *Extraction of Airways from CT 2009 (EXACT09)* website, that were used to compare different reconstruction approaches, as reported in [25]. It is known in [25] as CASE36 and it is a stack of dimension $512 \times 512 \times 315$ with voxel size $0.6 \times 0.6 \times 0.7$ mm. Dataset PA2 is a stack from Bellvitge Hospital (Barcelona) with dimension $370 \times 365 \times 239$ and with a voxel size of $0.76 \times 0.76 \times 0.8$ mm.

The results of case C36 obtained by our proposal can be compared with those reported in [25] and reproduced in Fig. 10. It

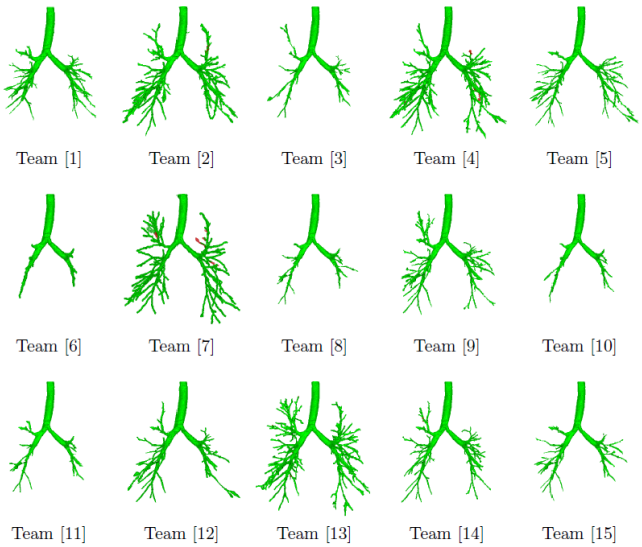

Figure 10: Results of CASE36 reported in EXACT '09 [25].

can be observed that the proposed approach has been able to reconstruct more bronchi than many others; and from those outperforming our proposal, some of them are not fully-automatic procedures. Also, for evaluation purposes, a manual reconstruction has been carried out for both datasets, C36 and PA2, to be used as ground truths (Fig. 9 bottom). The percentage (in volume) of reconstructed bronchi has been of 75% for case C36 and 79% for case PA2, and the percentage in length of 53% and 54% for C36 and PA2, respectively. Fig. 11 shows the skeletons for C36 used for this later comparison.

The proposed approach has been implemented using the AMIRA software with the Quantification+ option for the morphologic processing functions, in combination with Matlab. The computation times depend on the stack dimension, being the mean time around one hour on a standard computer. The most time-consuming stage is stage 2 and therefore it has been implemented using multicore tools for parallelization. The software is available at https://www.ioc.upc.edu/personal/jan.rosell/software.

6.2. Conclusions

The reconstruction of a 3D model of the tracheobronchial tree from the CT scans is a basic step for virtual bronchoscopy systems. The difficulty in the segmentation of bronchi (black regions in CT images) is due to the fact that airway walls do not appear clear enough because of partial volume effects and noise. In order to cope with this problem and try to reconstruct as much as possible the complete tracheobronchial tree including small bronchi, the paper has presented a proposal with the following main features:

1. *Detects the trachea and the main bronchi using a simple and robust method.* The trachea and the main bronchi are segmented using a region growing procedure with adaptive thresholds. It is a basic and not critical stage that aims to reduce computational time in the next stages of the whole process.

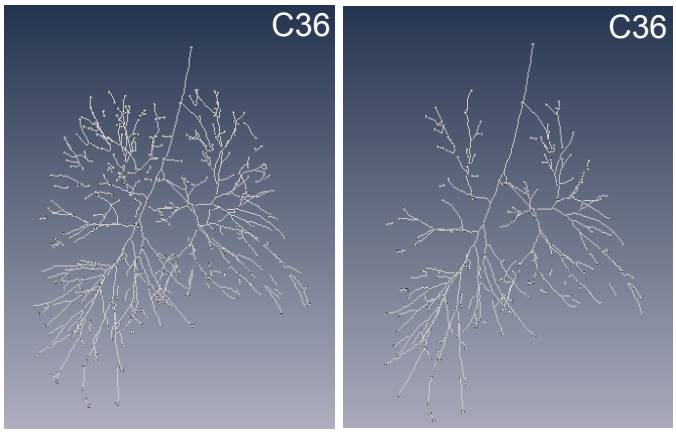

Figure 11: Skeletons of the ground truth (left) and of the reconstructed model (right) for the C36 case, used to compare the percentage (in length) of reconstructed bronchi.

2. *Focuses on bronchi wall detection in order to correctly segment thinner bronchi.* Any other potential airway region is detected by a simple segmentation process computed on an image where potential bronchi walls have been previously detected and enhanced. The procedure to detect bronchi walls is done using local gray-level pixel information and a method to detect and repair possible broken walls. The procedure is computationally expensive (although the implementation can be easily parallelized) but directly focuses on the problem of the partial volume effects and noise that make the airway walls to appear not clear enough, thus making it difficult to segment the airway regions.
3. *Possibility to connect any isolated bronchi to the main tree.* A method to connect isolated segmented regions to the main tree is provided as a last stage, based on path planning techniques. The method can take simultaneously into account in a simple and robust manner the directionality of the branches and the grayness of the connection.

In summary, the whole proposal is a conceptually simple method that does not rely on anatomical knowledge of the airway tree and that has few parameters easily set to correctly work with many different CT scans.

Current work is centered in improving the implementation to reduce the computational cost and also in including an automatic filtering procedure previous to the second stage in order to enhance its results.

References

[1] N. Shinagawa, K. Yamazaki, Y. Onodera, F. Asano, T. Ishida, H. Moriya, M. Nishimura, Virtual bronchoscopic navigation system shortens the examination time - feasibility study of virtual bronchoscopic navigation system, Lung Cancer 56 (2007) 201–206.

[2] R. C. Gonzalez, R. E. Woods, Digital Image Processing, Upper Saddle River, NJ, USA:Prentice Hall, 2002.

[3] R. M. Summers, D. H. Feng, S. M. Holland, M. Sneller, J. H. Shelhamer, Virtual bornchoscopy: segmentation method for real time display., Radiology 200 (1996) 857–862.

[4] K. Mori, J. Hasegawa, Y. Suenaga, J. Toriwaki, Automated anatomical labeling of the bronchial branch and its application to the virtual bronchoscopy system, Radiology 200 (1996) 857–862.

[5] T. Kitasaka, K. Mori, Y. Suenaga, J.-i. Hasegawa, J.-i. Toriwaki, A method for segmentng bronchial trees from 3D chest X-ray CT images, in: R. Ellis, T. Peters (Eds.), Medical Image Computing and Computer-Assisted Intervention - MICCAI 2003, volume 2879 of *Lecture Notes in Computer Science*, Springer Berlin Heidelberg, 2003, pp. 603–610.

[6] R. Pinho, R. Luyckx, J. Sijbers, Robust region growing based intrathoracic airway tree segmentation, Second International Workshop on Pulmonary Image Analysis (2009) 261–277.

[7] K. Lai, P. Zhao, Y. Huang, J. Liu, C. Wang, H. Feng, C. Li, Automatic 3D segmentation of lung airway tree: A novel adaptive region growing approach, in: Proceedings from 3rd International Conference on Biomedical and Bioinformatics Engineering, IEEE, 2009, pp. 1–4.

[8] D. Babin, E. Vansteenkiste, A. Pižurica, W. Philips, Segmentation of airways in lungs using projections in 3-D CT angiography images, in: Proceedings from 32nd Annual Conference of IEEE EMBS, volume I, IEEE, 2010, pp. 3162–3165.

[9] J. Serra, Image analysis and mathematical morphology, Orlando, FL, USA: Academic Press, Inc., 1982.

[10] Pisupati.C., L. Wolff, E. Zerhouni,W. Mitzner, Segmentation of 3D pulmonary tree using mathematical morphology. In: Mathematical Morphology and its Applications to Image and Signal Processing, Norwell, MA, USA: Kluwer AcademicPublishers, 1996, pp. 409–416.

[11] A. Fabijanska, Two-pass refion growing algorithm for segmenting airway tree from MDCT chest scans, Computerized Medical Imaging and Graphics 33 (2009) 537–546.

[12] B. Irving, P. Taylor, A. Todd-Pokropek, 3D segmentation of the airway tree using a morphology based method, in: Second International Workshop on Pulmonary Image Analysis, MICCAI, 2009, pp. 297–307.

[13] M. Sonka, W. Park, E. A. Hoffman, Rule-based detection of intrathoracic airway trees, IEEE Trans. on Medical Imaging 15 (1996) 314–326.

[14] W. Park, E. A. Hoffman, M. Sonka, Segmentation of intrathoracic airway trees: a fuzzy logic approach, IEEE Trans. on Medical Imaging 17 (1998) 489–497.

[15] J. Tschirren, E. A. Hoffman, G. McLennan, M. Sonka, Intrathoracic airway trees: Segmentation and airway morphology analysis from low-dose CT scans, IEEE Trans. on Medical Imaging 24 (2005) 1529–1539.

[16] B. Wang, P. K. Saha, J. K. Udupa, M. A. Ferrante, J. Baumgardner, D. A. roberts, R. R. Rizi, 3D airway segmentation via hyperpolarized ^{3}he gas mri by using scale-based fuzzy connectedness, Computerized Medical Imaging and Graphics 28 (2004) 77–86.

[17] C. Bauer, T. Pock, H. Bischof, R. Beichel, Airway tree reconstruction based on tube detection, in: Second International Workshop on Pulmonary Image Analysis, MICCAI, 2009, pp. 203–213.

[18] M. W. Graham, J. D. Gibbs, D. C. Cornish, W. E. Higgins, Robust 3-d airway tree segmentation for image-guided peripheral bronchoscopy, IEEE Trans. on Medical Imaging 29 (2010) 982–97.

[19] J. P. Carson, D. R. Einstein, K. R. Minard, M. V. Fanucchi, C. D. Wallis, R. A. Corley, Region-based geometric modelling of human airways and arterial vessels, Computerized Medical Imaging and Graphics 34 (2010) 572–578.

[20] S. Ding, Y. Ye, J. Tu, A. Subic, Refion-based geometric modelling of human airways and arterial vessels, Computerized Medical Imaging and Graphics 34 (2010) 114–121.

[21] P. Cabras, J. Rosell, A. Pérez, W. Aguilar, A. Rosell, Haptic based navigation for the virtual bronchoscopy, in: Proceedings from IFAC World Congress, volume 18, IFAC, 2011, pp. 9638–9643.

[22] J. Rosell, A. Pérez, P. Cabras, A. Rosell, Motion planning for the virtual bronchoscopy, in: Proc. of the Int. Conf. on Robotics and Automation, 2012, pp. 2932 – 2937.

[23] J.-C. Latombe, Robot Motion Planning., Norwell, MA, USA: Kluwer Academic Publishers, 1991.

[24] P. Cabras, J. Rosell, Using path planning techniques to improve airway tree segmentation from ct images, in: Proc. of the 6th Int. Conf. on Bio-inspired Systems and Signal Processing (BIOSIGNALS2013), 2013, pp. 189–195.

[25] P. Lo, B. van Ginneken, J. Reinhardt, M. de Bruijne, Extraction of airways from CT (EXACT'09), in: Second International Workshop on Pulmonary Image Analysis, MICCAI, 2009, pp. 175–189.